Applied Numerical Mathematics 162 (2021) 249–264

Contents lists available at ScienceDirect

Applied Numerical Mathematics

www.elsevier.com/locate/apnum

Numerical investigations of shallow water waves via generalized equal width (GEW) equation

Seydi Battal Gazi Karakoc [a,*], Khaled Omrani [b], Derya Sucu [a]

[a] Department of Mathematics, Faculty of Science and Art, Nevsehir Haci Bektas Veli University, Nevsehir, 50300, Turkey
[b] Institut Supérieur des Sciences Appliquées et de Technologie de Sousse, Sousse Ibn Khaldoun 4003, Université de Sousse, Tunisia

ARTICLE INFO

Article history:
Received 23 January 2020
Received in revised form 15 September 2020
Accepted 27 December 2020
Available online 5 January 2021

Keywords:
GEW equation
Galerkin finite element method
Semidiscrete Galerkin approximations
Crank Nicolson Galerkin method
Subdomain
Sextic B-spline

ABSTRACT

In this article, a mathematical model representing solution of the nonlinear generalized equal width (GEW) equation has been considered. Here we aim to investigate solutions of GEW equation using a numerical scheme by using sextic B-spline Subdomain finite element method. At first Galerkin finite element method is proposed and a priori bound has been established. Then a semi-discrete and a Crank-Nicolson Galerkin finite element approximation have been studied respectively. In addition to that a powerful Fourier series analysis has been performed and indicated that our method is unconditionally stable. Finally, proficiency and practicality of the method have been demonstrated by illustrating it on two important problems of the GEW equation including propagation of single solitons and collision of double solitary waves. The performance of the numerical algorithm has been demonstrated for the motion of single soliton by computing L_∞ and L_2 norms and for the other problem computing three invariant quantities I_1, I_2 and I_3. The presented numerical algorithm has been compared with other established schemes and it is observed that the presented scheme is shown to be effectual and valid.

1. Introduction

Nonlinear evolution equations (NLEEs) are a specific class of partial differential equations that have been investigated by many scientists for long to understand better about various real life problems. Especially, traveling wave solutions of such problems play a very important role in the study of PDE models arising from various natural phenomena, mathematical–physical sciences and engineering fields. For example, the wave phenomena appeared in fluid dynamics, solid state physics, optical fibers, nuclear physics, quantum mechanics, plasma physics, acoustic-gravity waves in compressible fluids, biology, nonlinear optics, chemical kinematics, chemical physics, etc [13]. Most known models of such real life phenomenon involving traveling waves are for instance the nonlinear Korteweg-de Vries (KdV) equation, regularized long wave (RLW) equation and equal width (EW) equation and so on. A wide range of such equations has been analyzed and several important computational algorithms have been proposed and developed to examine these types of models.

In this study, we aim to work on such an important nonlinear wave equation, the generalized equal width equation, of the form

$$U_t + \varepsilon U^p U_x - \mu U_{xxt} = 0, \tag{1}$$

* Corresponding author.
E-mail addresses: sbgk44@gmail.com (S.B.G. Karakoc), Khaled.Omrani@issatso.rnu.tn (K. Omrani), dryldrmsucu@gmail.com (D. Sucu).

https://doi.org/10.1016/j.apnum.2020.12.025
0168-9274/

where $U(x,t)$ is the wave amplitude of the water surface or a alike physical cardinality, $p \in \mathbb{Z}_+$, $\varepsilon > 0$ and $\mu > 0$ are parameters. Physical boundary conditions have need for $U \to 0$ as $|x| \to \infty$. Here the following reasonable physically meaningful restrictions have been imposed for (1)

$$\begin{aligned} &U(a,t)=0, \qquad U(b,t)=0, \\ &U_x(a,t)=0, \qquad U_x(b,t)=0, \\ &U_{xx}(a,t)=0, \qquad U_{xx}(b,t)=0, \quad t>0, \end{aligned} \tag{2}$$

$$U(x,0)=f(x), \quad a \le x \le b. \tag{3}$$

It is to note that U represents the negative of electrostatic potential in plasma treatments. So the solitary wave solution of (1) serves to better perceive the various physical phenomena with weak nonlinearity. It also includes dispersion waves for instance nonlinear transverse waves in shallow water, ion-acoustic and magneto-hydrodynamic waves in plasma and phonon packets in nonlinear crystals [26]. The PDE we study here is based on the EW equation and depends on both the generalized regularized long wave (GRLW) equation [28,29] and the generalized Korteweg-de Vries (GKdV) equation [16]. Studying GEW equation rigorously one may have the capability of analyzing the invention of secondary solitary waves and/or radiation to obtain insight into the corresponding procedures of particle physics [10,30]. The equation has many applications in physics and engineering [32]. For example, Eq. (1) represents the EW equation for $p=1$ which is an important model representing non-linear dispersive waves since it defines a large number of important physical phenomena [9,11,15,17,37,41]. Whereas, $p=2$ in (1) corresponds to the modified equal width (MEW) equation [5,7,12,18,19,21,25].

There are limited number of articles on the GEW equation available. Hamdi et al. [20] derived exact solitary wave solutions of the GEW equation. Whereas Evans and Raslan [14] studied the GEW equation by using the collocation method with quadratic B-spline at the midpoints. Also in another study, Raslan [34] studied GEW equation using cubic B-spline collocation scheme. Taghizadeh et al. [39] applied an extended homogeneous balance method to generate traveling wave solutions of the GEW equation. The GEW equation had been solved numerically by a meshless scheme based on a standard types of radial basis functions (RBFs) in [32] and a global collocation. Karakoc and Zeybek [26,42] implemented the lumped Galerkin cubic B-splines and a quintic B-spline collocation method with two types of linearization techniques. Petrov–Galerkin method for the problem targeted in this study is developed using a linear hat function as the test function and a quadratic B-spline as the trial function by Roshan [36].

To the best of our knowledge Subdomain finite element approach based on sextic B-splines to the GEW equation has not been applied before. Thus, in this article, we aim to develop a Subdomain finite element algorithm for the GEW equation using sextic B-splines. The rest of the article is arranged as follows:

- In Section 2, we discuss a Galerkin finite element scheme, semi-discrete Galerkin and Crank Nicolson Galerkin schemes for (1).
- Stability of the proposed scheme for (1) has been well studied in Section 3.
- Section 4 contains numerical experiments of traveling single solitary wave and interaction of two solitary waves with different types of initial and boundary conditions.
- We finish this study with some comments and conclusions in Section 5.

2. Galerkin finite element method

Similar to [6,23] we recall the initial boundary value problem (1) as

$$u_t - \mu u_{xxt} = \mathcal{F}_x(u), \tag{4}$$

where $\mathcal{F}(u) = -\frac{\varepsilon}{p+1}u^{p+1}$, depends on the initial and boundary conditions

$$u(x,0)=f_1(x), \quad a \le x \le b, \tag{5}$$

$$u(a,t)=0, \quad u(b,t)=0, \quad t>0. \tag{6}$$

Here we discuss some basic properties of solutions of (4) and review some basic theoretical bounds from [6]. We start here by discussing weak form of the solutions of (4) to that end. Denote $\Omega=(a,b)$, let $H^k(\Omega)$, $k \ge 0$ be a normed space over Ω and

$$H_0^k(\Omega) = \left\{ v \in H^k(\Omega) : D^i v = 0 \ \ on \ \ \partial\Omega, \ i=0, \ 1, \ \cdots, \ k-1 \right\} \tag{7}$$

where $D=\frac{\partial}{\partial x}$. Here $\|\cdot\|_k$ is considered as $H^k(\Omega)$ norm. The norm L^∞ is denoted by $\|\cdot\|_\infty$ and $\|\cdot\|_0 = \|\cdot\|$ symbolizes L^2 norm with $(\cdot,\cdot)$ symbolizes L^2 inner product. Taking L^2-inner product of (4) by ξ in $H_0^1(\Omega)$, and an application of simple calculus yields

$$(u_t,\xi) + \mu(Du_t, D\xi) = (D\mathcal{F}(u),\xi).$$

Our purpose here is to obtain $u(\cdot,t) \in H_0^1(\Omega)$ so that

$$(u_t, \xi) + \mu\,(Du_t, D\xi) = (D\mathcal{F}(u), \xi)\,,\ \forall\, \xi \in H_0^1(\Omega), \tag{8}$$

with $u(0) = u_0$. The existence and uniqueness of solutions of the weak form (8) has been well studied in [6,23,40].

Lemma 1. *If u is a weak solution of the inner product integrals (8) then*

$$\|u(t)\|_\infty \le C\|u_0\|_1,\ \textit{where } C \textit{ is a constant}. \tag{9}$$

Proof. Substituting $\xi = u$ in (8) yields

$$\frac{1}{2}\Big(\frac{d}{dt}\|u\|^2 + \mu\frac{d}{dt}\|Du\|^2\Big) = \int_\Omega uD\mathcal{F}(u)dx. \tag{10}$$

Noting that

$$uD\mathcal{F}(u) = D[u\mathcal{F}(u)] - D\psi(u),\ \text{ for } u \in H_0^1(\Omega),$$

where $\psi'(u) = \mathcal{F}(u)$. Also

$$\int_\Omega uD\mathcal{F}(u)dx = \int_\Omega D[u\mathcal{F}(u)]dx = 0, \tag{11}$$

as $u = 0$ on the boundary of the spatial domain Ω and $\psi(0) = 0$. It follows from (10) and (11) that

$$\frac{d}{dt}\|u\|^2 + \mu\frac{d}{dt}\|Du\|^2 = 0, \tag{12}$$

integrating (12) with respect to t, we obtain

$$\|u(t)\|^2 + \mu\|Du(t)\|^2 = \|u(0)\|^2 + \mu\|Du(0)\|^2.$$

By assumption μ is a positive constant, we have

$$\|u(t)\|_1^2 \le C\|u_0\|_1^2.$$

Thus applying Sobolev imbedding theorem one gets

$$\|u(t)\|_\infty \le C\|u_0\|_1.$$

The proof is completed. □

2.1. Semidiscrete Galerkin approximations

Suppose $u(t) \in H_0^1(\Omega) \cap H^{r+1}(\Omega)$, $r \ge 1$ for all $t \in [0,T]$, $h = \frac{b-a}{J}$ be the spatial step size and $x_i = ih$, $0 \le i \le J$, J is a given positive integer, be a regular mesh over $[a,b]$. Here S_h is considered to be a finite dimensional subspace of $H_0^1(\Omega)$ such that [8,40]

$$\inf_{\xi \in S_h}\{\|v - \xi\| + h\|D(v-\xi)\|\} \le Ch^{k+1}\|v\|_{k+1}, \tag{13}$$

for all $k \in \mathbb{Z}_+$ with $1 \le k \le r$ and $v \in H^{k+1}(\Omega)$ where C is a positive constant independent of h. For example

$$S_h = \Big\{v_h \in C^0(\overline{\Omega}),\quad v_h/_{[x_i,x_{i+1}]} \in \mathcal{P}_k,\ 0 \le i \le J-1,\ v_h(a) = v_h(b) = 0\Big\},$$

where $\mathcal{P}_k$ denotes the set of polynomials of degree $\le k$ [1].

Replacing u in (8) by $u_h : [0,T] \to S_h$ and integrating one gets

$$(u_{ht}, \xi) + \mu\,(Du_{ht}, D\xi) = -\,(\mathcal{F}(u_h), D\xi)\,,\ \ \forall\, \xi \in S_h, \tag{14}$$

where $u_h(0) = u_{0h} \in S_h$ is an appropriate approximation to u_0. Then we have the following a priori bound which follows from Lemma 1.

Lemma 2. *If u_h is a solution of (14) then*

$$\|u_h(t)\|_\infty \le C\|u_{0h}\|_1, \tag{15}$$

holds for some constant $C > 0$.

Next, we aim to estimate the error in the semi-discrete scheme (14). From now one the solution $u(x,t)$ of (1)–(3) and u_0 are sufficiently smooth. To facilitate the analysis an auxiliary projection $P_h : H_0^1(\Omega) \to S_h$ has been defined as follows:

$$\text{for } \ v \in H_0^1(\Omega), \qquad (D(P_h v - v), D\chi) = 0, \quad \forall \chi \in S_h. \tag{16}$$

Then (cf., for example, [3,4,6,8,24,40]) P_h satisfies the approximation properties:

Lemma 3. *If $u(x,t) \in C^1(0,T,H^{k+1}(\Omega))$ is the solution of (1)–(3) with $1 \le k \le r$, then*

$$\|u(t) - P_h u(t)\|_1 + \|u_t(t) - P_h u_t(t)\|_1 \le Ch^k, \tag{17}$$

where C is a constant independent of h.

For the proof of the statement, see [40] Lemma 1 page 6.
Now using the elliptic projection $P_h u$, we split the error $e = u_h - u$ as

$$e = u_h - u = (u_h - P_h u) + (P_h u - u) = \theta + \rho.$$

Then the following bound for e holds.

Theorem 1. *Let u_h be the solution of (14) and u be the solution of (1)–(3), u be sufficiently smooth, and the initial data satisfies $P_h u^0 = u_{0h}$. Then there exists a constant C independent of h such that*

$$\|u - u_h\|_\infty \le Ch^k.$$

Proof. Recall the error $u_h - u = \theta + \rho$, which has two parts. The estimates of the second part ρ are known from Lemma 3, and thus to find the bound for $\|u_h - u\|_\infty$, it is sufficient to estimate bound for θ. To that end subtracting (8) from (14) and using auxiliary projection, we obtain the following relation in θ

$$(\theta_t, \xi) + \mu\,(D\theta_t, D\xi) = (\mathcal{F}(u) - \mathcal{F}(u_h), D\xi) + \mu\,(D(u_t - P_h u_t), D\xi) + (u_t - P_h u_t, \xi)\,.$$

Now replacing ξ by θ in the above relation it yields

$$\begin{aligned}(\theta_t, \theta) + \mu\,(D\theta_t, D\theta) &= (\mathcal{F}(u) - \mathcal{F}(u_h), D\theta) + \mu\,(D(u_t - P_h u_t), D\theta) + (u_t - P_h u_t, \theta)\\ &\le \|\mathcal{F}(u) - \mathcal{F}(u_h)\|\|D\theta\| + \mu\|D\rho_t\|\|D\theta\| + \|\rho_t\|\|\theta\|.\end{aligned}$$

Applying Lipschitz condition on $\mathcal{F}$ and then (17) it follows that

$$\|\mathcal{F}(u) - \mathcal{F}(u_h)\| \le C(\|\rho\| + \|\theta\|).$$

Therefore,

$$\frac{d}{dt}\|\theta\|_1^2 \le C(\|\theta\|_1^2 + \|\rho\|_1^2 + \|\rho_t\|_1^2).$$

Integrating with respect to time from 0 to t, we obtain

$$\|\theta(t)\|_1^2 \le \|\theta(0)\|_1^2 + C\int_0^t \Big(\|\rho(s)\|_1^2 + \|\rho_t(s)\|_1^2\Big)dt, \text{ applying Gronwall's inequality,}$$

since by assumption we assumed that $P_h u^0 = u_{0h}$ i.e. $\theta(0) = P_h u^0 - u_{0h} = 0$. It follows from Lemma 3 that

$$\|\theta(t)\|_1 \le Ch^k.$$

An application of Sobolev imbedding Theorem yields

$$\|\theta(t)\|_\infty \le Ch^k.$$

Using Lemma 3 along with triangle inequality, we complete the rest of the proof. □

2.2. Crank Nicolson Galerkin scheme (CNGS)

Here we focus on to analyze a fully discrete scheme for the GEW equation. For spatial integration we use standard Galerkin method and for the time integration the Crank–Nicolson scheme has been used. In fact we motivate ourselves to get solution of the semi-discrete problem (14) in $[0, T]$, $T > 0$. Let N be a positive full number and $\Delta t = \frac{T}{N}$ in order that $t^n = n\Delta t$, $n = 0, 1, \cdots, N$. Now we take into consideration that [43]

$$\phi^n = \phi(t^n), \quad \phi^{n-1/2} = \frac{\phi^n + \phi^{n-1}}{2}, \quad \partial_t \phi^n = \frac{\phi^n - \phi^{n-1}}{\Delta t}.$$

We write a time discretized Galerkin algorithm using above notations with

$$\left(\partial_t U^n, \xi\right) + \mu\left(D\partial_t U^n, D\xi\right) = -\left(\mathcal{F}(U^{n-1/2}), D\xi\right), \quad \forall \xi \in S_h, \tag{18}$$

with $U^0 = u_{0h}$, where $u_{0h} \in S_h$ is an appropriate approximation of u_0. To derive accuracy results for the CNGS (18), the following a priori bound is useful.

Lemma 4. *Let U^n be the solution of (18), then $\exists$ a constant C that does not dependent of h and k such that $\|U^n\|_\infty \le C\|U^0\|_1$ holds.*

Proof. Substituting $\xi = U^{n-1/2}$ in (18), one obtains

$$\frac{1}{2}\partial_t \|U^n\|^2 + \mu\frac{1}{2}\partial_t \|DU^n\|^2 = -\left(\mathcal{F}(U^{n-1/2}), DU^{n-1/2}\right) = 0.$$

So

$$\|U^n\|^2 + \mu\|DU^n\|^2 = \|U^{n-1}\|^2 + \mu\|DU^{n-1}\|^2 = \cdots = \|U^0\|^2 + \mu\|DU^0\|^2.$$

Therefore,

$$\|U^n\|_1^2 \le C\|U^0\|_1^2,$$

where C is a constant. From the Sobolev imbedding theorem

$$\|U^n\|_\infty^2 \le C\|U^n\|_1^2 \le C\|U^0\|_1^2,$$

we obtain the desired estimate. □

It is our motto now to estimate the error in CNGS, thus, we use the error decomposition with $u^n = u(t^n)$

$$U^n - u^n = (U^n - P_h u^n) + (P_h u^n - u^n) = \theta^n + \rho^n.$$

Theorem 2. *Let U^n be the solution of (18) and u be that of (1)–(3). There exists a constant C independent of h and Δt such that*

$$\|U^n - u^n\|_\infty \le C(h^k + (\Delta t)^2),$$

where h, Δt sufficiently small, if $P_h u^0 = u_{0h}$ holds and u is considered to be sufficiently smooth.

Proof. As of the semi-discrete case the estimate of ρ^n follows from Lemma 3, thus estimation for θ^n is only required now to proof the result. Using the (8), (16) and (18) we have the following relation for θ^n

$$\begin{aligned}(\partial_t \theta^n, \xi) + \mu(D\partial_t \theta^n, D\xi) = &\left(\mathcal{F}(u^{n-1/2}) - \mathcal{F}(U^{n-1/2}), D\xi\right) - (\partial_t \rho^n, \xi) \\ &+ (w^n, \xi) + \mu(Dw^n, D\xi) - \mu(D\partial_t \rho^n, D\xi),\end{aligned} \tag{19}$$

where $w^n = u_t(t^{n-1/2}) - \partial_t u^n$. Using Taylor's formula, we have

$$\|w^n\|_1 \le C(\Delta t)^3 \int_{t_{n-1}}^{t_n} \|u_{ttt}(s)\|_1^2 ds. \tag{20}$$

Now applying Lipschitz condition on $\mathcal{F}$ and the limitedness of $\|U^n\|_\infty$ and $\|u^n\|_\infty$, it is easy to see that

$$\|\mathcal{F}(u^{n-1/2}) - \mathcal{F}(U^{n-1/2})\| \le C(\|\rho^{n-1/2}\| + \|\theta^{n-1/2}\|). \tag{21}$$

Choosing $\xi = \theta^{n-1/2}$ in (19) and using (20) and (21), we obtain

$$\begin{aligned}\|\partial_t\theta^n\|_1^2 \le\ & C\Big[\|\theta^{n-1/2}\|_1\|D\theta^{n-1/2}\| + \|\rho^{n-1/2}\|_1\|D\theta^{n-1/2}\| + \|\partial_t\rho^n\|\|\theta^{n-1/2}\| \\ & +\|D\partial_t\rho^n\|\|D\theta^{n-1/2}\| + \|w^n\|\|\theta^{n-1/2}\| + \|Dw^n\|\|D\theta^{n-1/2}\|\Big].\end{aligned} \tag{22}$$

This implies that

$$\|\partial_t\theta^n\|_1^2 \le C\Big(\|\theta^n\|_1^2 + \|\theta^{n-1}\|_1^2\Big) + CR_n,$$

where

$$R_n = \|\rho^n\|_1^2 + \|\rho^{n-1}\|_1^2 + \|\partial_t\rho^n\|_1^2 + \|w^n\|_1^2.$$

Therefore,

$$(1 - C\Delta t)\|\theta^n\|_1^2 \le (1 + C\Delta t)\|\theta^{n-1}\|_1^2 + C\Delta t R_n.$$

Choosing Δt sufficiently small so that $(1 - C\Delta t) > 0$, we obtain

$$\|\theta^n\|_1^2 \le \Big(\frac{1 + C\Delta t}{1 - C\Delta t}\Big)\|\theta^{n-1}\|_1^2 + \Big(\frac{C\Delta t}{1 - C\Delta t}\Big)R_n.$$

After repeated application, we obtain

$$\|\theta^n\|_1^2 \le \Big(\frac{1 + C\Delta t}{1 - C\Delta t}\Big)^n\|\theta^0\|_1^2 + C\Delta t\sum_{j=1}^{n}\Big(\frac{1 + C\Delta t}{1 - C\Delta t}\Big)^{n-j}R_j \le C\|\theta^0\|_1^2 + C\Delta t\sum_{j=1}^{n}R_j.$$

From Lemma 3, we have

$$\|\theta^n\|_1 \le C(h^k + (\Delta t)^2).$$

An application of the Sobolev Imbedding theorem yields

$$\|\theta^n\|_\infty \le C(h^k + (\Delta t)^2).$$

Using the triangle inequality with estimates of ρ^n, we complete the rest of the proof. □

3. Sextic B-splines and analysis of the Subdomain method

In this part of our study, we aim to approximate the nonlinear GEW Eq. (4)–(5) using following over-specified boundary conditions

$$\begin{aligned}&u(a,\ t) = 0, \quad u(b,\ t) = 0,\\ &\tfrac{\partial u}{\partial x}(a,\ t) = 0, \quad \tfrac{\partial u}{\partial x}(b,\ t) = 0,\\ &\tfrac{\partial^2 u}{\partial x^2}(a,\ t) = 0, \quad \tfrac{\partial^2 u}{\partial x^2}(b,\ t) = 0, \quad t > 0.\end{aligned} \tag{23}$$

To approximate solutions over the interval $[a,\ b]$ partition $a = x_0 < x_1 < \ldots < x_N = b$ of the space sub-interval is considered distributed uniformly with step size $h = \frac{b-a}{N}$, $m = 0, 1, 2, \cdots, N$. Here $\phi_m(x)$ are sextic B-splines at the knot points x_m. We follow Prenter [33] to define sextic B-splines $\phi_m(x)$, $(m = -3, -2, -1, \ldots, N, N+1, N+2)$ at the points x_m

$$\phi_m(x) = \frac{1}{h^6}\begin{cases}(x - x_{m-3})^6, & x \in [x_{m-3}, x_{m-2}],\\ (x - x_{m-3})^6 - 7(x - x_{m-2})^6, & x \in [x_{m-2}, x_{m-1}],\\ (x - x_{m-3})^6 - 7(x - x_{m-2})^6 + 21(x - x_{m-1})^6, & x \in [x_{m-1}, x_m],\\ (x - x_{m-3})^6 - 7(x - x_{m-2})^6 + 21(x - x_{m-1})^6 - 35(x - x_m)^6, & x \in [x_m, x_{m+1}],\\ (x - x_{m+4})^6 - 7(x - x_{m+3})^6 + 21(x - x_{m+2})^6, & x \in [x_{m+1}, x_{m+2}],\\ (x - x_{m+4})^6 - 7(x - x_{m+3})^6, & x \in [x_{m+2}, x_{m+3}],\\ (x - x_{m+4})^6, & x \in [x_{m+3}, x_{m+4}],\\ 0\,, & otherwise.\end{cases} \tag{24}$$

Using the basis functions defined above, $U_N(x,t)$ is defined by

$$U_N(x,t) = \sum_{j=-3}^{N+2}\phi_j(x)\delta_j(t), \tag{25}$$

where the parameters $\delta_j(t)$ are employed using boundary and weighted residual conditions. U_m, U'_m, U''_m and U'''_m at the knots x_m can be calculated from (25) and sextic B-splines (24) in the following form

$$\begin{aligned}
U_m &= U(x_m) = \delta_{m-3} + 57\delta_{m-2} + 302\delta_{m-1} + 302\delta_m + 57\delta_{m+1} + \delta_{m+2},\\
U'_m &= U'(x_m) = \tfrac{6}{h}(-\delta_{m-3} - 25\delta_{m-2} - 40\delta_{m-1} + 40\delta_m + 25\delta_{m+1} + \delta_{m+2}),\\
U''_m &= U''(x_m) = \tfrac{30}{h^2}(\delta_{m-3} + 9\delta_{m-2} - 10\delta_{m-1} - 10\delta_m + 9\delta_{m+1} + \delta_{m+2}),\\
U'''_m &= U'''(x_m) = \tfrac{120}{h^3}(-\delta_{m-3} - \delta_{m-2} + 8\delta_{m-1} - 8\delta_m + \delta_{m+1} + \delta_{m+2}).
\end{aligned} \tag{26}$$

Using the equality

$$h\eta = x - x_m, \quad 0 \le \eta \le 1, \tag{27}$$

the finite interval $[x_m,\ x_{m+1}]$ is transformed into more easily practicable interval $[0,\ 1]$. In this case, the sextic B-splines (24) in variable η over $[0,\ 1]$ can be written as [22]:

$$\phi^e = \begin{cases}
\phi_{m-3} = 1 - 6\eta + 15\eta^2 - 20\eta^3 + 15\eta^4 - 6\eta^5 + \eta^6,\\
\phi_{m-2} = 57 - 150\eta + 135\eta^2 - 20\eta^3 - 45\eta^4 + 30\eta^5 - 6\eta^6,\\
\phi_{m-1} = 302 - 240\eta - 150\eta^2 + 160\eta^3 + 30\eta^4 - 60\eta^5 + 15\eta^6,\\
\phi_m = 302 + 240\eta - 150\eta^2 - 160\eta^3 + 30\eta^4 + 60\eta^5 - 20\eta^6,\\
\phi_{m+1} = 57 + 150\eta + 135\eta^2 + 20\eta^3 - 45\eta^4 - 30\eta^5 + 156\eta^6,\\
\phi_{m+2} = 1 + 6\eta + 15\eta^2 + 20\eta^3 + 15\eta^4 + 6\eta^5 - 6\eta^6,\\
\phi_{m+3} = \eta^6.
\end{cases} \tag{28}$$

Sextic B-splines apart from $\phi_{m-3}(x)$, $\phi_{m-2}(x)$, $\phi_{m-1}(x)$, $\phi_m(x)$, $\phi_{m+1}(x)$, $\phi_{m+2}(x)$ and $\phi_{m+3}(x)$ are zero over the domain $[0, 1]$. Therefore approximation (25) over the element parameters $\delta_{m-3}, \delta_{m-2}, \delta_{m-1}, \delta_m, \delta_{m+1}, \delta_{m+2}, \delta_{m+3}$ is written as

$$U_N(\eta, t) = \sum_{j=m-3}^{m+3} \delta_j(t)\phi_j(\eta) \tag{29}$$

where $\phi_{m-3}(x), \phi_{m-2}(x), \phi_{m-1}(x), \phi_m(x), \phi_{m+1}(x)$, $\phi_{m+2}(x)$ and $\phi_{m+3}(x)$ act as element shape functions [2].

Finite element methods belong to the class of weighted residual methods [31]. It is a scheme to approximate solutions of various types of most classes of differential equations. By the way, subdomain method is one of the standard methods. In the subdomain method, one divides a physical domain into a number of non-overlapping subdomains [38]. Number of subdomain n is considered same as the number of unknown coefficients in the approximating function. For example, for one-dimensional problems,

$$W_m(x) = \begin{cases} 1, & x \in [x_m,\ x_{m+1}],\\ 0, & otherwise, \end{cases} \qquad m = 1, 2, \cdots, n\ . \tag{30}$$

In weighted residual method, one may write

$$\int_a^b W_m R(x)dx = \int_{x_m}^{x_{m+1}} R(x)dx = 0. \tag{31}$$

This property guarantees that the average of the residual over all the sub-domains $[x_m, x_{m+1}]$ is forced to be zero [38]. Applying subdomain finite element method (SFEM) to (1) with weight function (30), it is easy to obtain the integral form of (1) as

$$\int_{x_m}^{x_{m+1}} 1 \cdot (U_t + \varepsilon U^p U_x - \mu U_{xxt})dx = 0. \tag{32}$$

Implementing the transformation (27) in (32) and integrating (32) term by term and using some manipulation by parts, brings along [37]

$$\begin{aligned}
&\frac{h}{7}(\dot\delta_{m-3} + 120\dot\delta_{m-2} + 1191\dot\delta_{m-1} + 2416\dot\delta_m + 1191\dot\delta_{m+1} + 120\dot\delta_{m+1} + \dot\delta_{m+3})\\
&+ Z_m(-\delta_{m-3} - 56\delta_{m-2} - 245\delta_{m-1} + 245\delta_{m+1} + 56\delta_{m+2} + \delta_{m+3})\\
&- \frac{4\mu}{h}(-\dot\delta_{m-3} - 25\dot\delta_{m-2} - 40\dot\delta_{m-1} + 40\dot\delta_m + 25\dot\delta_{m+1} + \dot\delta_{m+2}) = 0,
\end{aligned} \tag{33}$$

where $\dot{\delta} = \frac{d\delta}{dt}$ and

$$Z_m = \varepsilon(\delta_{m-3} + 57\delta_{m-2} + 302\delta_{m-1} + 302\delta_m + 57\delta_{m+1} + \delta_{m+2})^p. \tag{34}$$

Changing $\dot{\delta}$ by $\dot{\delta} = \frac{\delta^{n+1}-\delta^n}{\Delta t}$ and the parameter δ by $\delta = \frac{1}{2}(\delta^n + \delta^{n+1})$, the system (33) turns into the

$$\begin{aligned} &\omega_{m1}\delta_{m-3}^{n+1} + \omega_{m2}\delta_{m-2}^{n+1} + \omega_{m3}\delta_{m-1}^{n+1} + \omega_{m4}\delta_{m}^{n+1} + \omega_{m5}\delta_{m+1}^{n+1} + \omega_{m6}\delta_{m+2}^{n+1} + \omega_{m7}\delta_{m+3}^{n+1} \\ &= \omega_{m7}\delta_{m-3}^{n+1} + \omega_{m6}\delta_{m-2}^{n+1} + \omega_{m5}\delta_{m-1}^{n+1} + \omega_{m4}\delta_{m}^{n+1} + \omega_{m3}\delta_{m+1}^{n+1} + \omega_{m2}\delta_{m+2}^{n+1} + \omega_{m1}\delta_{m+3}^{n+1} \end{aligned} \tag{35}$$

where

$$\begin{aligned} &\omega_{m1} = 1 - EZ_m - M, \qquad \omega_{m2} = 120 - 56EZ_m - 24M, \\ &\omega_{m3} = 1191 - 245EZ_m - 15M, \quad \omega_{m4} = 2416 + 80M, \\ &\omega_{m5} = 1191 + 245EZ_m - 15M, \quad \omega_{m6} = 120 + 56EZ_m - 24M, \\ &\omega_{m7} = 1 + EZ_m - M, \quad E = \frac{7\Delta t}{2h}, \quad M = \frac{42\mu}{h^2}, \quad m = 0, 1, \cdots, N-1. \end{aligned} \tag{36}$$

Here (35) is a system of N linear equations with $(N+6)$ unknown parameters $(\delta_{-3}, \delta_{-2}, ..., \delta_{N+1}, \delta_{N+2})$. Six additional limitations are required to find δ_i's uniquely. Imposing BCs (2) to the system (35), we may remove $\delta_{-3}, \delta_{-2}, \delta_{-1}, \delta_N, \delta_{N+1}$ and δ_{N+2} from the system (35) which then becomes a system with N unknowns

$$Md^{n+1} = Nd^n$$

where

$$d = (\delta_0, \delta_1, ..., \delta_{N-1}).$$

A lumped form of Z_m is computed as $\left(\frac{U_m+U_{m+1}}{2}\right)^p$ and

$$Z_m = \frac{\varepsilon}{2^p}(\delta_{m-3} + 58\delta_{m-2} + 359\delta_{m-1} + 604\delta_m + 359\delta_{m+1} + 58\delta_{m+2} + \delta_{m+3})^p. \tag{37}$$

The resulting system can be solved by using a modified form of Thomas algorithm [35] and in this procedure an inner iteration is also employed at each time step to reduce the non-linearity. Consequently, we derive the following two levels n and $n+1$ relationship relating δ_m^{n+1} and δ_m^n:

$$\begin{aligned} &\varkappa_1\delta_{m-3}^{n+1} + \varkappa_2\delta_{m-2}^{n+1} + \varkappa_3\delta_{m-1}^{n+1} + \varkappa_4\delta_{m}^{n+1} + \varkappa_5\delta_{m+1}^{n+1} + \varkappa_6\delta_{m+2}^{n+1} + \varkappa_7\delta_{m+3}^{n+1} \\ &= \varkappa_7\delta_{m-3}^{n} + \varkappa_6\delta_{m-2}^{n} + \varkappa_5\delta_{m-1}^{n} + \varkappa_4\delta_{m}^{n} + \varkappa_3\delta_{m+1}^{n} + \varkappa_2\delta_{m+2}^{n} + \varkappa_1\delta_{m+3}^{n} \end{aligned} \tag{38}$$

where

$$\begin{aligned} &\varkappa_1 = \alpha - \beta - \lambda, \qquad \varkappa_2 = 120\alpha - 56\beta - 24\lambda, \qquad \varkappa_3 = 1191\alpha - 245\beta - 15\lambda, \\ &\varkappa_4 = 2416\alpha + 80\beta, \quad \varkappa_5 = 1191\alpha + 245\beta - 15\lambda, \quad \varkappa_6 = 120\alpha + 56\beta - 24\lambda, \\ &\varkappa_7 = \alpha + \beta - \lambda \end{aligned}$$

and

$$\alpha = 1, \quad \beta = EZ_m, \quad \lambda = M, \quad m = 0, 1, ..., N-1. \tag{39}$$

In order to solve the system (38), one necessarily need to evaluate the initial values δ^0 by using $U(x,0) = f(x)$ and

$$\begin{aligned} &U_N(x_m, 0) = U(x_m, 0), \qquad U_N^{'}(a,0) = U_N^{'}(b,0) = 0, \\ &U_N^{''}(a,0) = U_N^{''}(b,0) = 0, \quad U_N^{'''}(a,0) = U_N^{'''}(b,0) = 0, \end{aligned}$$

and a simplification yields a following $N \times N$ system for δ_m^0:

$$\begin{bmatrix} 384 & 312 & 24 & & & & & & & & \\ \frac{2681}{9} & 358 & \frac{568}{9} & 1 & & & & & & & \\ \frac{512}{9} & 303 & \frac{2719}{9} & 57 & 1 & & & & & & \\ & 1 & 57 & 302 & 302 & 57 & 1 & & & & \\ & & & & & & & 1 & 57 & \frac{2719}{9} & 303 & \frac{512}{9} \\ & & & & & & & & 1 & \frac{568}{9} & 358 & \frac{2681}{9} \\ & & & & & & & & & 24 & 312 & 384 \end{bmatrix} \begin{bmatrix} \delta_0^0 \\ \delta_1^0 \\ \delta_2^0 \\ \cdot \\ \cdot \\ \delta_{N-3}^0 \\ \delta_{N-2}^0 \\ \delta_{N-1}^0 \end{bmatrix} = \begin{bmatrix} U(x_0,0) \\ U(x_1,0) \\ U(x_2,0) \\ \cdot \\ U(x_{N-3},0) \\ U(x_{N-2},0) \\ U(x_{N-1},0) \end{bmatrix}.$$

3.1. Stability analysis

Here we motivate ourself to study stability of the scheme briefly. To that end, it is suitable to use the Fourier method based on the Von-Neumann theory where the growth factor of Fourier mode is defined as

$$\delta_j^n = g^n e^{ijkh} \tag{40}$$

where $k =$ mode number and $h =$ element size and $i = \sqrt{-1}$. It is to note that Fourier method can not be applied to the nonlinearity $U^p U_x$. And thus we linearize by presuming U^p a local constant such as Z_m [27]. If the equality (40) is substituted into (38) and use of some simplifications yields

$$g = \frac{A - iB}{A + iB}, \tag{41}$$

where

$$\begin{aligned} A &= 1208 + 40\lambda + (1191 - 15\lambda)\cos(kh) + (120 - 24\lambda)\cos(2kh) + (1 - \lambda)\cos(3kh), \\ B &= 245\beta \sin(kh) + 56\beta \sin(2kh) + \beta \sin(3kh). \end{aligned} \tag{42}$$

Here it is evident that $|g| = 1$, and thus by the von Neumann necessary criterion it guarantees that the linearized scheme is neutrally stable.

4. Computational experiments

In this section we illustrate numerical scheme described in previous sections by calculating propagation of single solitary waves and the interaction of solitons for the GEW equation. For this purpose we consider homogenous boundary conditions only. We measure error in such an approximation by

$$L_2 = \left\| U^{exact} - U_N \right\|_2 \simeq \sqrt{h \sum_{j=0}^{N} \left| U_j^{exact} - (U_N)_j \right|^2},$$

and

$$L_\infty = \left\| U^{exact} - U_N \right\|_\infty \simeq \max_j \left| U_j^{exact} - (U_N)_j \right|.$$

The exact solution of GRLW IBVP is given by [32,42]

$$U(x,t) = \sqrt[p]{\frac{c(p+1)(p+2)}{2\varepsilon} \sec h^2[\frac{p}{2\sqrt{\mu}}(x - ct - x_0)]}$$

and that has a solitary wave of amplitude $\sqrt[p]{\frac{c(p+1)(p+2)}{2\varepsilon}}$, wave speed c, width $\frac{p}{2\sqrt{\mu}}$ and it is initially centered at x_0. The conservation properties of the GEW equation mean conservation of mass, momentum and energy. These there properties are guaranteed by computing following three invariants [14,26,34]

$$I_1 = \int_{-\infty}^{\infty} U(x,t)dx, \quad I_2 = \int_{-\infty}^{\infty} [U^2(x,t) + \mu U_x^2(x,t)]dx, \quad I_3 = \int_{-\infty}^{\infty} U^{p+2}(x,t)dx. \tag{43}$$

After computing solitary wave motion, we observe I_1, I_2 and I_3 values to verify the accuracy of the proposed computational numerical algorithm.

4.1. Dispersion of a single solitary wave

In order to exemplify the validity of our numerical algorithm, we conceive the first case of a single soliton solution for the parameters $p = 2$, $h = 0.1$, $c = 0.5$, $\Delta t = 0.2$, $\varepsilon = 3$, $\mu = 1$, $x_0 = 30$ over the region $[0, 80]$ to compare with that of earlier works [26,36,42]. These parameters generate the amplitude 1.0 and the simulations are performed to time $t = 20$. Note that $I_1 = 3.1415927$, $I_2 = 2.6666667$ and $I_3 = 1.3333333$ are considered as exact values of the invariants [26,36,42]. We report the values of the error norms and invariants for different time levels in Table 1. The table predicates that the three conserved quantities remain nearly stable as the time progress and the changes of the quantities are also in good agreement with their analytic values. A comparison with analytic solution as well as the approximated values in [26,36,42] has been done and presented in Table 2 for $t = 20$. It is observed that although our error norms are greater than that given in [36], our error norms are less than or almost same with [26,42]. Fig. 1 illustrates the approximate solutions at different

Table 1
Numerical values of invariants and error norms for $p = 2$.

Time	I_1	I_2	I_3	L_2	L_∞
0	3.1415863	2.6666616	1.3333283	0.00000000	0.00000000
5	3.1415875	2.6666629	1.3333292	0.00518887	0.00334528
10	3.1415875	2.6666627	1.3333290	0.01020620	0.00638295
15	3.1415873	2.6666624	1.3333287	0.01517519	0.00942302
20	3.1415870	2.6666621	1.3333284	0.02014034	0.01246335

Table 2
Comparison of invariants and error norms for $p = 2$, at $t = 20$.

Method	I_1	I_2	I_3	L_2	L_∞
Analytic	3.1415961	2.6666667	1.3333333	0.00000000	0.00000000
Our Method	3.1415870	2.6666621	1.3333284	0.02014034	0.01246335
Cubic Galerkin [26]	3.1589605	2.6902580	1.3570299	0.03803037	0.02629007
Quintic Collocation First Scheme [42]	3.1250343	2.6445829	1.3113394	0.05132106	0.03416753
Quintic Collocation Second Scheme [42]	3.1416722	2.6669051	1.3335718	0.01675092	0.01026391
Petrov-Galerkin [36]	3.14159	2.66673	1.33341	0.0123326	0.0086082

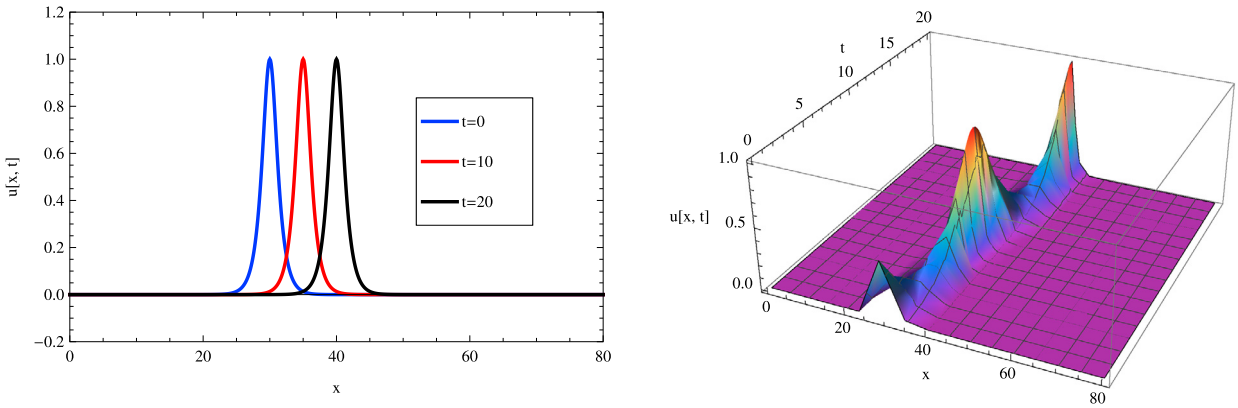

Fig. 1. Single solitary wave profiles at $t = 0, 10, 20$ for $p = 2$. (For interpretation of the colors in the figure(s), the reader is referred to the web version of this article.)

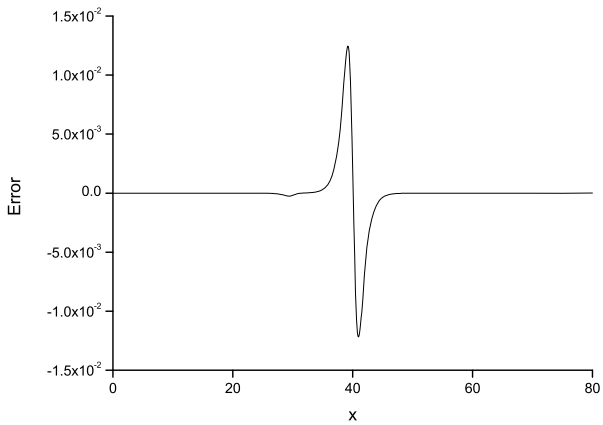

Fig. 2. Error graph corresponding to the parameters of Table 1 at $t = 20$.

t values. One may notice from illustrations that the studied scheme performs the motion of propagation of a solitary wave preserves amplitude and shape [27]. To demonstrate the approximation errors we plot computational error at time $t = 20$ in Fig. 2.

Then we start to illustrate the scheme considering $p = 3$, $h = 0.1$, $c = 0.3$, $\Delta t = 0.2$, $\mu = 1$, $\varepsilon = 3$, $x_0 = 30$ over the spatial domain $[0, 80]$. For these set of parameters the amplitude $u = 1.0$ at time $t = 20$. Invariant quantities and error norms are illustrated in Table 3. It is to notice from Table 3 that the computational errors for the proposed scheme are

Table 3
Numerical values of invariants and error norms for $p = 3$.

Time	I_1	I_2	I_3	L_2	L_∞
0	2.8043580	2.4639101	0.9855618	0.00000000	0.00000000
5	2.8043574	2.4639093	0.9855610	0.00373796	0.00248800
10	2.8043572	2.4639089	0.9855606	0.00749284	0.00498955
15	2.8043569	2.4639086	0.9855603	0.01126141	0.00749175
20	2.8043567	2.4639082	0.9855599	0.01503316	0.00999356

Table 4
Comparison of invariants and error norms for $p = 3$, at $t = 20$.

Method	I_1	I_2	I_3	L_2	L_∞
Our Method	2.8043567	2.4639082	0.9855599	0.01503316	0.00999356
Cubic Galerkin [26]	2.8187398	2.4852249	1.0070200	0.01655637	0.01370453
Quintic Collocation First Scheme [42]	2.8043570	2.4639086	0.9855602	0.00801470	0.00538237
Quintic Collocation Second Scheme [42]	2.8042943	2.4637495	0.9854011	0.00708553	0.00480470
Petrov-Galerkin [36]	2.80436	2.46389	0.98556	0.00484271	0.00370926

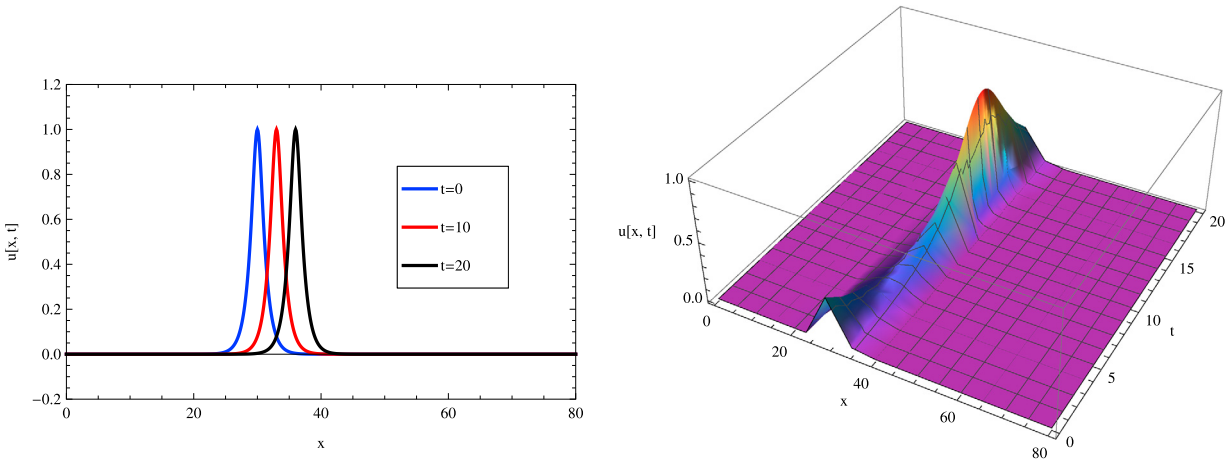

Fig. 3. Single solitary wave profiles at $t = 0, 10, 20$ for $p = 3$.

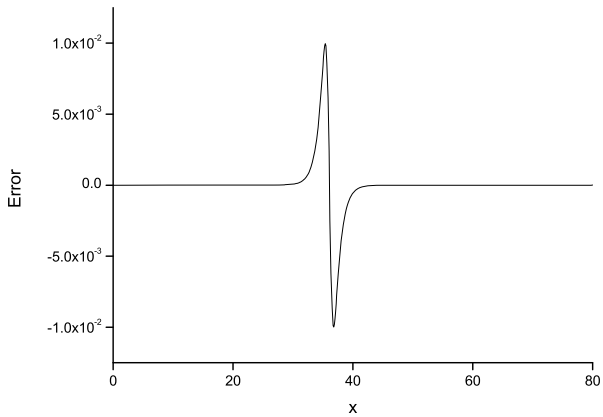

Fig. 4. Error graph corresponding to the parameters of Table 3 at $t = 20$.

adequately small and our invariance tests confirm them almost to be constants as time increases. In Table 4 we compare the invariants and error norms computed by the present method with those of [26,36,42] at $t = 20$. It is observed that outcomes presented by us here are better than that of [26] and are compatible at the same with the others. Fig. 3 shows the motion of solitary wave at $t = 0$, $t = 10$, $t = 20$. It is observed from the graphics that the solutions generated by the presented method preserve the properties (amplitude and shape). Numerical error distribution is depicted at time $t = 20$ in Fig. 4. The error deviates from -10^{-2} to 10^{-2} and the maximum of it occurs around the central position of solitary wave.

Table 5
Numerical values of invariants and error norms for $p = 4$.

Time	I_1	I_2	I_3	L_2	L_∞
0	2.6220516	2.3561915	0.7853952	0.00000000	0.00000000
5	2.6220468	2.3561845	0.7853880	0.00352271	0.00250308
10	2.6220458	2.3561835	0.7853870	0.00707776	0.00502744
15	2.6220458	2.3561835	0.7853870	0.01066843	0.00755428
20	2.6220458	2.3561835	0.7853869	0.01427724	0.00908006

Table 6
Comparison of invariants and error norms for $p = 4$, at $t = 20$.

Method	I_1	I_2	I_3	L_2	L_∞
Our Method	2.6220458	2.3561835	0.7853869	0.01427724	0.00908006
Cubic Galerkin [26]	2.6327833	2.3730032	0.8023383	0.00890617	0.00821991
Quintic Collocation First Scheme [42]	2.6220508	2.3561901	0.7853939	0.00421697	0.00297952
Quintic Collocation First Scheme [42]	2.6219284	2.3559327	0.7851364	0.00339086	0.00247031
Petrov-Galerkin [36]	2.62206	2.35615	0.78534	0.00230499	0.00188285

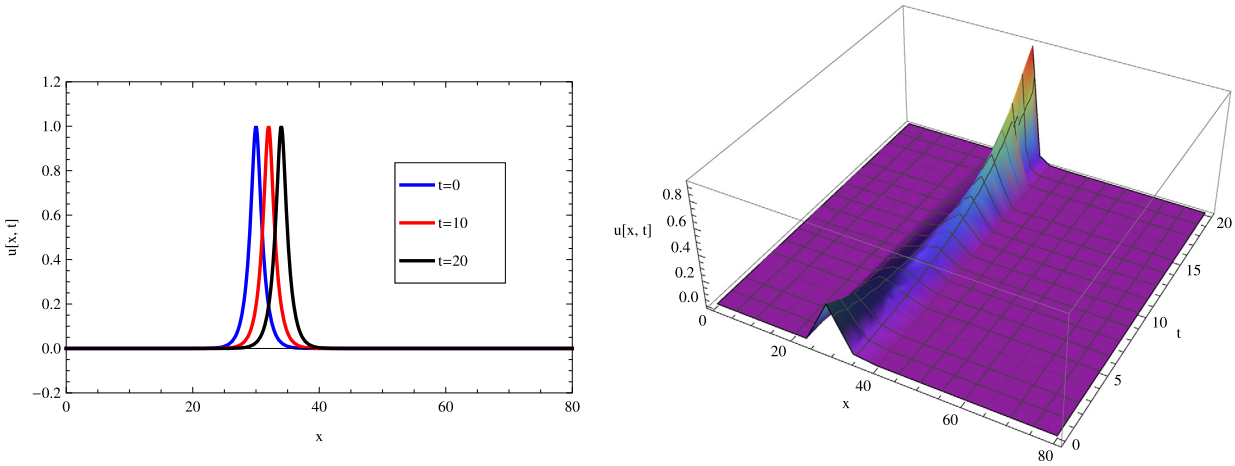

Fig. 5. Single solitary wave profiles at $t = 0, 10, 20$ for $p = 4$.

As a final illustration we set $p = 4$, $h = 0.1$, $c = 0.2$, $\Delta t = 0.2$, $\mu = 1$, $\varepsilon = 3$, $x_0 = 30$ and $x \in [0, 80]$ to compare with that of [26,36,42]. These set of parameters generate the amplitude $u = 1.0$ at time $t = 20$. The computed results are presented in Table 5. The table shows that values of the error norms are sufficiently small and invariants quantities are computationally constant as $t > 0$ progresses. Hence method presented here is acceptably conservative. The comparison between the results obtained by us with those of [26,36,42] is also exhibited in Table 6. It is noticed from the Table 6 that although error norm L_2 is higher but our error norm L_∞ is comparable to others. The behaviors of solutions for $c = 0.2$, $h = 0.1$, $p = 4$, $\Delta t = 0.2$ at times $t = 0$, $t = 10$ and $t = 20$ are shown in Fig. 5. One may observe that the solitary wave moves to the right at a constant velocity and remains its shape and amplitude. Error at time $t = 20$ has been presented in Fig. 6. It is evident that the maximum errors lie between -10^{-2} to 10^{-2} and max errors remain around the central position of the solitary wave.

4.2. Interaction of two solitary waves

Now we move onto studying two solitary waves this test problem. Here we focus on to study interaction of two solitary waves considering

$$U(x,0) = \sum_{j=1}^{2} \sqrt[p]{\frac{c_j(p+1)(p+2)}{2\varepsilon} sech^2[\frac{p}{2\sqrt{\mu}}(x - x_j)]}, \tag{44}$$

where c_1, c_2, x_1, and x_2 are arbitrary constants. $U(x, 0)$ defined by (44) guarantees two solitary waves at the same direction and have different amplitudes. In our numerical experiment, we choose three sets of parameters by varying p, c_i and keep $h = 0.1$, $\varepsilon = 3$, $\Delta t = 0.025$, $\mu = 1$ same and consider $0 \le x \le 80$.

Fixing $c_1 = 0.5$, $c_2 = 0.125$ and $p = 2$ we illustrate I_1, I_2 and I_3 at $t = 0$ to $t = 60$ in Table 7. It is clear that the computed values of I_1, I_2 and I_3 are nearly constant during all the computations and compatible with those in [26,36,42]. A graphical

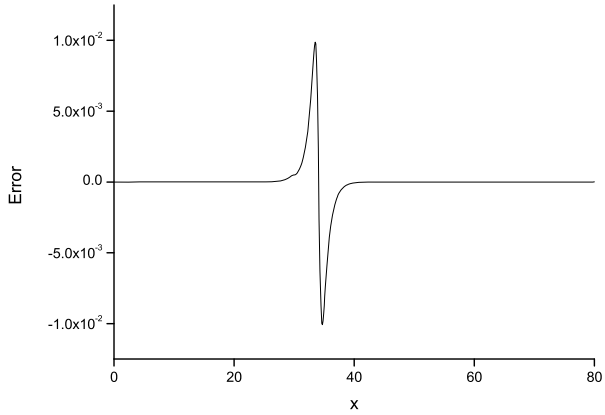

Fig. 6. Error graph corresponding to the parameters of Table 5 at $t = 20$.

Table 7
Numerical values of invariants for collision of two solitary waves with $p = 2$.

	t	0	20	40	60
	Our Method	4.20653	4.20654	4.20654	4.20654
I_1	[26]	4.20653	4.20653	4.20616	4.20490
	[42] First	4.20653	4.20653	4.20653	4.20653
	[42] Second	4.20653	4.20653	4.20653	4.20653
	[36]	4.20655	4.20655	4.20655	4.20655
	Our Method	3.07989	3.07989	3.07990	3.07990
I_2	[26]	3.07987	3.07991	3.07947	3.07777
	[42] First	3.07988	3.07988	3.07988	3.07988
	[42] Second	3.07988	3.07988	3.07988	3.07988
	[36]	3.07977	3.07980	3.07987	3.07974
	Our Method	1.01636	1.01637	1.01637	1.01638
I_3	[26]	1.01636	1.01638	1.01654	1.01616
	[42] First	1.01636	1.01636	1.01636	1.01636
	[42] Second	1.01636	1.01636	1.01636	1.01636
	[36]	1.01634	1.01634	1.01634	1.01633

Table 8
Numerical values of invariants for collision of two solitary waves with $p = 3$.

	t	0	30	60	90	100
	Our Method	4.20653	4.20650	4.20614	4.20486	4.20498
I_1	[26]	4.20653	4.20653	4.20616	4.20490	4.20503
	[42] First	4.20653	4.20653	4.20653	4.20653	4.20653
	[42] Second	4.20653	4.20653	4.20653	4.20653	4.20653
	[36]	4.20655	4.20655	4.20655	4.20655	4.20655
	Our Method	3.07988	3.07985	3.07961	3.07872	3.07881
I_2	[26]	3.07987	3.07991	3.07947	3.07777	3.07797
	[42] First	3.07988	3.07988	3.07988	3.07988	3.07988
	[42] Second	3.07988	3.07988	3.07988	3.07988	3.07988
	[36]	3.97977	3.07980	3.07987	3.07974	3.07972
	Our Method	1.01636	1.01632	1.01646	1.01619	1.01619
I_3	[26]	1.01636	1.01638	1.01654	1.01616	1.01616
	[42] First	1.01636	1.01636	1.01636	1.01636	1.01636
	[42] Second	1.01636	1.01636	1.01636	1.01636	1.01636
	[36]	1.01634	1.01634	1.01634	1.01633	1.01634

representation of two solitary wave formation has been confirmed in Fig. 7 and Fig. 8. For the second experiment, we select parameters $c_1 = 0.3$, $c_2 = 0.0375$ and $p = 3$ and the computations are continued till $t = 100$ to compare I_1, I_2 and I_3 which have been demonstrated in Table 8. It is noticed from this tabular data that the quantities are once again marginally constant and compatible with [26,36,42]. We also demonstrate the time evolution of solutions in Fig. 9. It confirms the preservations of solitary waves.

For the last case, to allow the interaction of two solitary waves we have selected the parameters $c_1 = 0.2$, $c_2 = 1/80$, $p = 4$ and $t \in (0, 120]$. The computer generated outcomes have been presented in Table 9. The results agree with that from

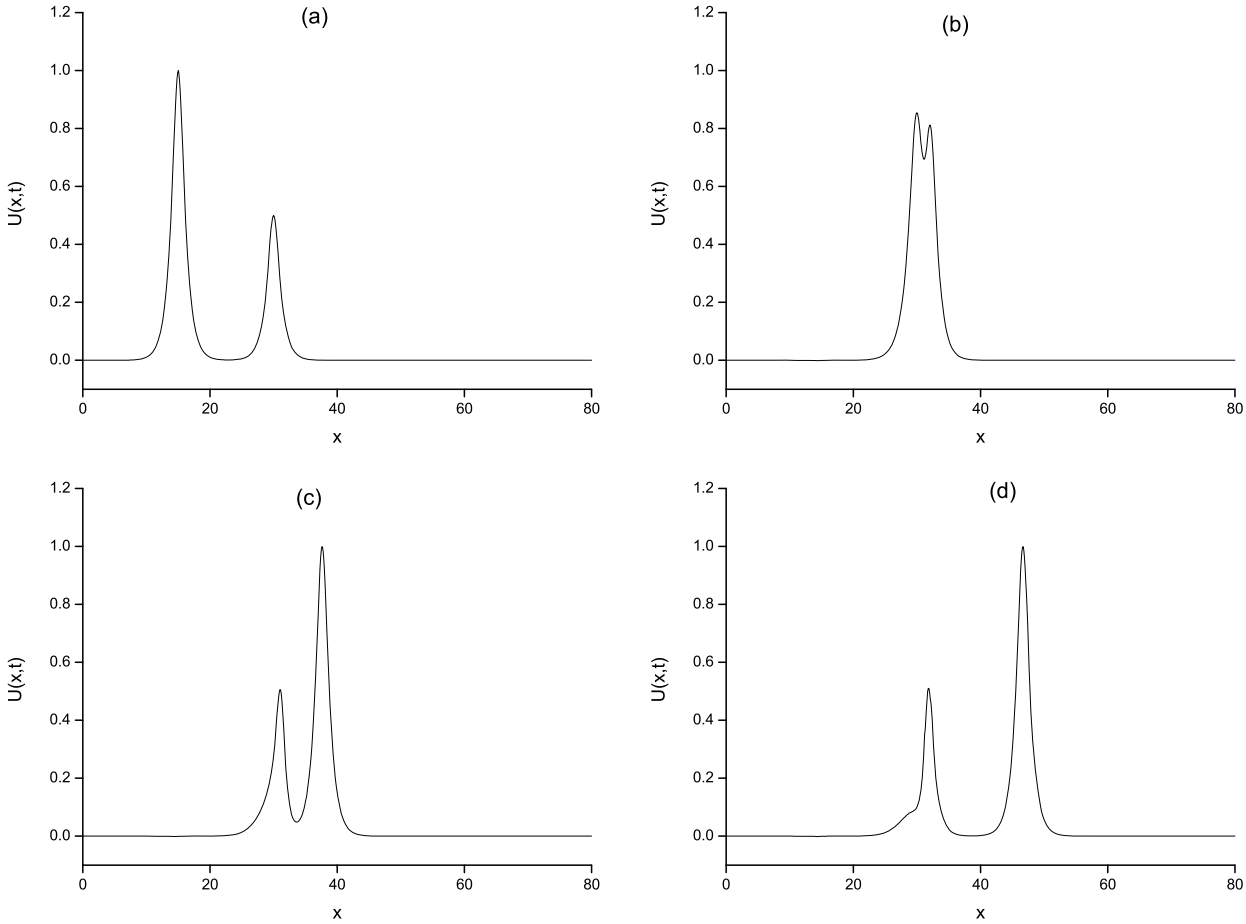

Fig. 7. Collision of two solitary waves at $p = 2$; (a) $t = 0$, (b) $t = 20$, (c) $t = 40$, (d) $t = 60$.

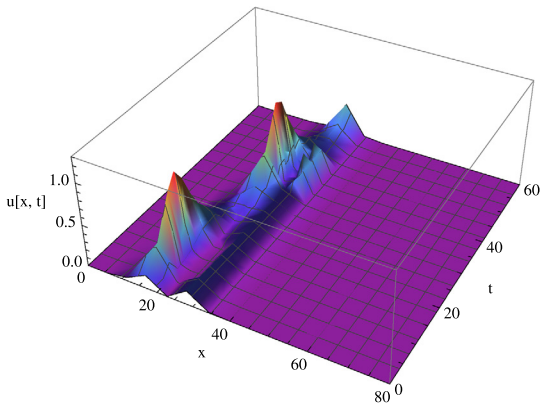

Fig. 8. Collision of two solitary waves at $p = 2$, a three dimensional illustration of the same.

[26,36,42]. We illustrate the dynamical changes of solutions over varying t in Fig. 10 which guarantees the efficiency of the scheme presented here.

5. Conclusion

This study is based on sextic B-spline functions, a Subdomain approach has been well studied and implemented considering GEW equations with some fixed choices initial and boundary conditions. Firstly the proposed method has been presented and a priori bound is analyzed. Then a semi-discrete scheme and a full discrete (Crank-Nicolson scheme) scheme

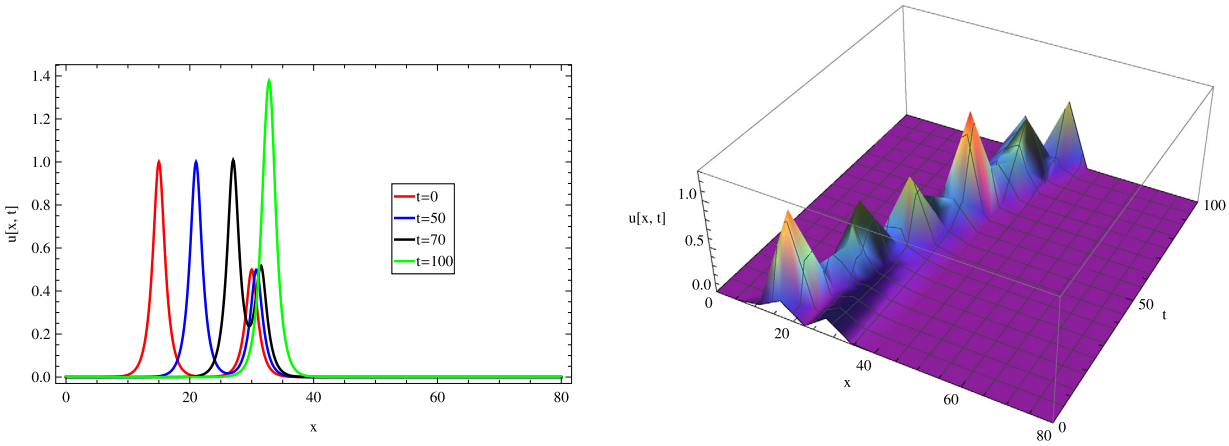

Fig. 9. Collision of two solitary waves at $p = 3$.

Table 9
Numerical values of invariants for collision of two solitary waves with $p = 4$.

	t	0	30	60	90	120
	Our Method	3.93307	3.93303	3.93379	3.93216	3.93018
I_1	[26]	3.93307	3.93309	3.93388	3.93222	3.93026
	[42] First	3.93307	3.93307	3.93307	3.93307	3.93307
	[42] Second	3.93307	3.93307	3.93307	3.93307	3.93307
	[36]	3.93309	3.93309	3.93309	3.93309	3.93308
	Our Method	2.94979	2.94518	2.94618	2.94461	2.94323
I_2	[26]	2.94524	2.94527	2.94703	2.94436	2.94212
	[42] First	2.94524	2.94524	2.94524	2.94524	2.94524
	[42] Second	2.94524	2.94523	2.94523	2.94523	2.94523
	[36]	2.94512	2.94510	2.94505	2.94520	2.94511
	Our Method	0.79766	0.79761	0.79871	0.79803	0.79788
I_3	[26]	0.79766	0.79770	0.79942	0.79812	0.79794
	[42] First	0.79766	0.79766	0.79766	0.79766	0.79766
	[42] Second	0.79766	0.79766	0.79766	0.79766	0.79766
	[36]	0.797614	0.797612	0.797622	0.797612	0.797611

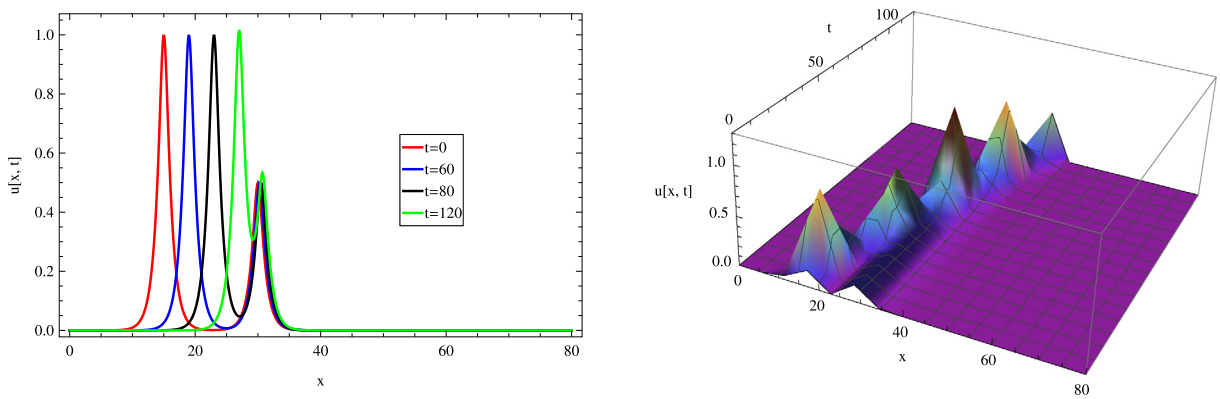

Fig. 10. Collision of two solitary waves at $p = 4$.

are analyzed respectively. For the Crank-Nicolson Galerkin finite element scheme, the spatial discretization is based on the standard Galerkin method, and the Crank-Nicolson scheme is used for the temporal integration. We use a linearization to analyze stability. In our study we confirm that our linearized numerical scheme is unconditionally stable. Also we have implemented the algorithm through single solitary wave and two solitary waves. Accuracy of the scheme has been tested in both the L_2 and L_∞ error norms and by computing I_1, I_2 and I_3. The exemplified outcomes confirm that our error norms are good enough as required and they outperform most contemporary numerical calculations or they are compatible with the best result in existing literature. Thus it guarantees that our comprehensive algorithm is efficient and powerful and it works well for dynamic PDEs.

References

[1] T. Achouri, A fully Galerkin method for the damped generalized regularized long-wave (DGRLW) equation, Numer. Methods Partial Differ. Equ. 25 (2009) 668–684.
[2] T. Ak, S.B.G. Karakoc, H. Triki, Numerical simulation for treatment of dispersive shallow water waves with Rosenau-KdV equation, Eur. Phys. J. Plus 131 (2016) 356–370.
[3] M.N. Ali, S.M. Husnine, A. Saha, S.K. Bhowmik, S. Dhawan, T. Ak, Exact solutions, conversation laws, bifurcation of nonlinear and supernonlinear travelling waves for Sharma-Tasso-Olyver equation, Nonlinear Dyn. 94 (2018) 1791–1801.
[4] N. Atouani, K. Omrani, Galerkin finite element method for the Rosenau-RLW equation, Comput. Math. Appl. 66 (2013) 289–303.
[5] S.K. Bhowmik, Piecewise polynomial approximation of a nonlocal phase transitions model, Math. Anal. Appl. 420 (2014) 1069–1094.
[6] S.K. Bhowmik, S.B.G. Karakoc, Numerical solutions of the generalized equal width wave equation using Petrov Galerkin method, Appl. Anal. (2019) 1–19.
[7] S.K. Bhowmik, R. Belbakib, T.Z. Boulmezaoud, S. Mziou, Solving two dimensional second order elliptic equations in exterior domains using the inverted finite elements method, Comput. Math. Appl. 72 (2014) 2315–2333.
[8] P.G. Ciarlet, Finite Element Methods for Elliptic Problems, Society for Industrial and Applied Math., 2002.
[9] I. Dag, B. Saka, A cubic B-spline collocation method for the EW equation, Math. Comput. Appl. 9 (2004) 381–392.
[10] R.K. Dodd, J.C. Eilbeck, J.D. Gibbon, H.C. Morris, Solitons and Nonlinear Wave Equations, Academic Press, 1982.
[11] A. Esen, A numerical solution of the equal width wave equation by a lumped Galerkin method, Appl. Math. Comput. 168 (2005) 270–282.
[12] A. Esen, A lumped Galerkin method for the numerical solution of the modified equal-width wave equation using quadratic B-splines, Int. J. Comput. Math. 83 (2006) 449–459.
[13] A. Esfahani, On the generalized Kadomtsev–Petviashvili equation with generalized evolution and variable coefficients, Phys. Lett. A 374 (2010) 3635–3645.
[14] D.J. Evans, K.R. Raslan, Solitary waves for the generalized equal width (GEW) equation, Int. J. Comput. Math. 82 (2005) 445–455.
[15] L.R.T. Gardner, G.A. Gardner, Solitary waves of the equal width wave equation, J. Comput. Phys. 101 (1991) 218–223.
[16] L.R.T. Gardner, G.A. Gardner, T. Geyikli, The boundary forced MKdV equation, J. Comput. Phys. 11 (1994) 5–12.
[17] L.R.T. Gardner, G.A. Gardner, F.A. Ayoup, N.K. Amein, Simulations of the EW undular bore, Commun. Numer. Methods Eng. 13 (1997) 583–592.
[18] T. Geyikli, S.B.G. Karakoc, Septic B-spline collocation method for the numerical solution of the modified equal width wave equation, Appl. Math. 2 (2011) 739–749.
[19] T. Geyikli, S.B.G. Karakoc, Subdomain finite element method with quartic B-splines for the modified equal width wave equation, Comput. Math. Math. Phys. 55 (2015) 410–421.
[20] S. Hamdi, W.H. Enright, W.E. Schiesser, J.J. Gottlieb, Exact solutions of the generalized equal width wave equation, in: Proceedings of the International Conference on Computational Science and Its App., vol. 2668, 2003, pp. 725–734.
[21] S.B.G. Karakoc, Numerical solutions of the modified equal width wave equation with finite elements method, Ph.D. Thesis, Inonu University, 2011.
[22] S.B.G. Karakoc, T. Ak, Numerical solution of Rosenau-KdV equation using subdomain finite element method, New Trends Math. Sci. 4 (2016) 223–235.
[23] S.B.G. Karakoc, S.K. Bhowmik, Numerical approximation of the generalized regularized long wave equation using Petrov-Galerkin finite element method, Numer. Methods Partial Differ. Equ. 35 (2019) 2236–2257.
[24] S.B.G. Karakoc, S.K. Bhowmik, Galerkin finite element solution for Benjamin–Bona–Mahony–Burgers equation with cubic B-splines, Comput. Math. Appl. 77 (2019) 1917–1932.
[25] S.B.G. Karakoc, T. Geyikli, Numerical solution of the modified equal width wave equation, Int. J. Differ. Equ. 2012 (2012) 1–15.
[26] S.B.G. Karakoc, H. Zeybek, A cubic B-spline Galerkin approach for the numerical simulation of the GEW equation, Stat. Optim. Inf. Comput. 4 (2016) 30–41.
[27] S.B.G. Karakoc, N.M. Yagmurlu, Y. Ucar, Numerical approximation to a solution of the modified regularized long wave equation using quintic B-splines, Bound. Value Probl. (2013) 1–27.
[28] D. Kaya, A numerical simulation of solitary-wave solutions of the generalized regularized long wave equation, Appl. Math. Comput. 149 (2004) 833–841.
[29] D. Kaya, S.M. El-Sayed, An application of the decomposition method for the generalized KdV and RLW equations, Chaos Solitons Fractals 17 (2003) 869–877.
[30] J.C. Lewis, J.A. Tjon, Resonant production of solitons in the RLW equation, Phys. Lett. A 73 (1979) 275–279.
[31] L.E. Lindgren, From Weighted Residual Methods to Finite Element Methods, 2009.
[32] H. Panahipour, Numerical simulation of GEW equation using RBF collocation method, Commun. Numer. Anal. (2012) 1–28.
[33] P.M. Prenter, Splines and Variational Methods, John Wiley Sons, NY, USA, 1975.
[34] K.R. Raslan, Collocation method using cubic B-spline for the generalised equal width equation, Int. J. Simul. Process Model. 2 (2006) 37–44.
[35] D.U. Von Rosenberg, Methods for Solution of Partial Differential Equation, American Elsevier Publishing Inc., 1969.
[36] T. Roshan, A Petrov–Galerkin method for solving the generalized regularized equal width (GEW) equation, J. Comput. Appl. Math. 235 (2011) 1641–1652.
[37] B. Saka, A finite element method for equal width equation, Appl. Math. Comput. 175 (2006) 730–747.
[38] A. Salih, Weighted Residual Methods, Department of Aerospace Engineering Indian Institute of Space Science and Technology, Thiruvananthapuram, 2016.
[39] N. Taghizadeh, M. Mirzazadeh, M. Akbari, M. Rahimian, Exact solutions for generalized equal width equation, Math. Sci. Lett. 2 (2013) 99–106.
[40] V. Thomee, Springer Ser. Comput. Math. (2006).
[41] S.I. Zaki, A least-squares finite element scheme for the EW equation, Comput. Methods Appl. Mech. Eng. 189 (2000) 587–594.
[42] H. Zeybek, S.B.G. Karakoc, Application of the collocation method with B-splines to the GEW equation, Electron. Trans. Numer. Anal. 46 (2017) 71–88.
[43] Y.D. Zhang, Y.M. Zhao, F.L. Wang, Y.F. Tang, High-accuracy finite element method for 2D time fractional diffusion-wave equation on anisotropic meshes, Int. J. Comput. Math. 95 (2018) 218–230.